χ_1 Torsion Angle Dynamics in Proteins from Dipolar Couplings

Anthony Mittermaier and Lewis E. Kay*

Contribution from the Protein Engineering Centers of Excellence and the Departments of Medical Genetics, Biochemistry and Chemistry, University of Toronto, Toronto, Ontario, Canada M5S 1A8

Received March 5, 2001. Revised Manuscript Received April 30, 2001

Abstract: Experiments are presented for the measurement of one-bond carbon−proton dipolar coupling values at CH and CH_2 positions in ^{13}C-labeled, ∼50% fractionally deuterated proteins. $^{13}C^{\beta}-^{1}H^{\beta}$ dipolar couplings have been measured for 38 of 49 possible residues in the 63-amino-acid B1 domain of peptostreptococcal protein L in two aligning media and interpreted in the context of side-chain χ_1 torsion angle dynamics. The β protons for 18 of the 25 β-methylene-containing amino acids for which dipolar data are available can be unambiguously stereoassigned, and for those residues which are best fit to a single rotamer model the χ_1 angles obtained deviate from crystal structure values by only 5.2° (rmsd). The results for 11 other residues are significantly better fit by a model that assumes jumps between the three canonical ($\chi_1 \approx -60°$, 60°, 180°) rotamers. Relative populations of the rotamers are determined to within ±6% uncertainty on average and correlate with dihedral angles observed for the three molecules in the crystal asymmetric unit. Entropic penalties for quenching χ_1 jumps are considered for six mobile residues thought to be involved in binding to human immunoglobulins. This study demonstrates that dipolar couplings may be used to characterize both the conformation of static residues and side-chain motion with high precision.

Introduction

NMR studies of macromolecules can provide dynamic information spanning a large range of time scales.[1,2] Motions with time constants on the order of picoseconds to nanoseconds can be explored by spin relaxation techniques, providing a description of the amplitude and frequencies of bond librations,[3] larger scale backbone and side-chain dynamics,[4−6] and, in some cases, domain rearrangements.[7] Slower dynamics (microsecond to millisecond time scale) can be probed by measuring the excess contribution to relaxation from chemical exchange processes via relaxation dispersion experiments.[8,9] Still slower processes (on the time scale of seconds) can be studied by NOESY-type experiments or by monitoring the exchange of multispin coherences and spin orders.[10−12]

Complementary dynamic information can be provided by measuring vicinal scalar coupling constants and intraresidue NOEs.[13−17] For example, fluctuations of the χ_1 torsion angle can be probed on a per-residue basis by analyzing $^{3}J_{\alpha\beta}$ coupling constants in concert with the relative intensities of intraresidue NOEs involving the α and the two β protons. Additional information can be obtained from intraresidue $^{13}C'-^{1}H^{\beta}$, $^{13}C'-^{13}C^{\gamma}$, $^{15}N-^{1}H^{\beta}$, and $^{15}N-^{13}C^{\gamma}$ scalar coupling constants.[18] In a recent study of side-chain dynamics in unfolded states, Yang et al. have combined measurements of $^{13}C^{\beta}-^{1}H^{\beta}$ dipole−dipole cross-correlated relaxation and intraresidue $^{15}N-^{13}C^{\gamma}$ and $^{13}C'-^{13}C^{\gamma}$ couplings to produce a picture of χ_1 torsion angle dynamics in an unfolded SH3 domain.[19] In related work, Schwalbe and co-workers have measured $^{15}N-^{13}C^{\gamma}$ and $^{13}C'-^{13}C^{\gamma}$ couplings in denatured hen lysozyme as a probe of side-chain conformation in unfolded states.[20]

A quantitative measure of dynamics using an approach based on scalar couplings requires accurate parameterizations of ^{3}J as a function of χ_1. Although the development of powerful triple-resonance experiments in the past few years has greatly increased both the number of couplings that can be measured and their accuracy,[18] parameterization of the appropriate Karplus relationships,[21] nevertheless, remains challenging. For example, Karplus curves are generated by combining measured scalar

(1) Kay, L. E. *Nat. Struct. Biol. NMR Suppl.* **1998**, *5*, 513−516.
(2) Ishima, R.; Torchia, D. A. *Nat. Struct. Biol.* **2000**, *7*, 740−743.
(3) Palmer, A. G.; Williams, J.; McDermott, A. *J. Phys. Chem.* **1996**, *100*, 13293−13310.
(4) Muhandiram, D. R.; Yamazaki, T.; Sykes, B. D.; Kay, L. E. *J. Am. Chem. Soc.* **1995**, *117*, 11536−11544.
(5) LeMaster, D. M.; Kushlan, D. M. *J. Am. Chem. Soc.* **1996**, *118*, 9255−9264.
(6) Wand, A. J.; Urbauer, J. L.; McEvoy, R. P.; Bieber, R. J. *Biochemistry* **1996**, *35*, 6116−6125.
(7) Tjandra, N.; Kuboniwa, H.; Ren, H.; Bax, A. *Eur. J. Biochem.* **1995**, *230*, 1014−1024.
(8) Loria, J. P.; Rance, M.; Palmer, A. G. *J. Am. Chem. Soc.* **1998**, *121*, 2331−2332.
(9) Mulder, F. A. A.; van Tilborg, P. J. A.; Kaptein, R.; Boelens, R. *J. Biomol. NMR* **1999**, *13*, 275−288.
(10) Montelione, G. T.; Wagner, G. *J. Am. Chem. Soc.* **1989**, *111*, 3096−3098.
(11) Wider, G.; Neri, D.; Wüthrich, K. *J. Biomol. NMR* **1991**, *1*, 93−98.
(12) Farrow, N. A.; Zhang, O.; Forman-Kay, J. D.; Kay, L. E. *J. Biomol. NMR* **1994**, *4*, 727−734.
(13) Dzakula, Z.; Edison, A. S.; Westler, W. M.; Markely, J. L. *J. Am. Chem. Soc.* **1992**, *114*, 6200−6207.
(14) Dzakula, Z.; Westler, W. M.; Edison, A. S.; Markley, J. L. *J. Am. Chem. Soc.* **1992**, *114*, 6195−6199.
(15) Spyracopoulos, L.; Gagne, S. M.; Gronwald, W.; Kay, L. E.; Sykes, B. D. In *NMR studies of protein sidechain dynamics*; Jardetzky, O., Ed.; Plenum Press: New York, 1998.
(16) Clore, G. M.; Gronenborn, A. M. *Crit. Rev. Biochem. Mol. Biol.* **1989**, *24*, 479−557.
(17) Montelione, G. T.; Winkler, M. E.; Rauhenbuehler, P.; Wagner, G. *J. Magn. Reson.* **1989**, *82*, 198−204.
(18) Bax, A.; Vuister, G. W.; Grzesiek, S.; Delaglio, F.; Wang, A. C.; Tschudin, R.; Zhu, G. *Methods Enzymol.* **1994**, *239*, 79−105.
(19) Yang, D.; Mok, Y. K.; Muhandiram, D. R.; Forman-Kay, J. D.; Kay, L. E. *J. Am. Chem. Soc.* **1999**, *121*, 3555−3556.
(20) Hennig, M.; Bermel, W.; Spencer, A.; Dobson, C. M.; Smith, L. J.; Schwalbe, H. *J. Mol. Biol.* **1999**, *288*, 705−723.
(21) Karplus, M. *J. Chem. Phys.* **1959**, *30*, 11−15.

10.1021/ja010595d CCC: $20.00
Published on Web 06/19/2001

coupling values with dihedral angles extracted from an X-ray structure. This approach assumes that the solution and crystal forms of the protein are identical, an almost certain oversimplification. Incorporating the effects of conformational averaging into the parameterization is difficult when the extent of the dynamics is not known a priori. In addition, a single average set of parameters describing ^3J vs χ_1 is obtained for all residues, which ignores substituent effects. Recent MD/DFT studies by Case and Brüschweiler[22] and experimental work by Schmidt and co-workers[23] address some of the limitations discussed above in the context of couplings for measurement of ϕ,ψ dihedral angles in proteins. However, to our knowledge, studies have not appeared which discuss these issues in the context of couplings for the measurement of side-chain dihedral angles.

In this paper we investigate the use of residual dipolar couplings as a probe of torsion angle dynamics in proteins. These couplings can be measured to high accuracy using triple-resonance pulse schemes and are exquisitely sensitive to the orientation of individual bond vectors in the molecular alignment frame. Moreover, like scalar couplings, dipolar couplings are sensitive to motions over a broad spectrum of time scales ranging from picosecond to nanosecond dynamics to motions with time constants on the order of tens of milliseconds (so long as the frequencies of the motions exceed the magnitudes of the dipolar couplings).[24] Methods for measuring $^{13}C-^1H$ dipolar couplings in methylene groups in proteins are presented, and $^{13}C^\beta-^1H^\beta$, $^{13}C^\alpha-^1H^\alpha$, $^{13}C^\alpha-^{13}C'$, and $^{13}C^\alpha-^{13}C^\beta$ couplings are determined for many amino acids in the 63-residue B1 immunoglobulin binding domain of peptostreptococcal protein-L[25] using two different alignment media. For several residues implicated in mediating the interaction between protein-L and Ig κ light chains,[26] significantly better agreement between measured and predicted $^{13}C^\beta-^1H^\beta$[2,3] dipolar couplings is obtained when a model which includes rotamer jumps is used. A detailed characterization of side-chain dynamics is likely to be important for understanding the energetics of this binding event.

Materials and Methods

Protein Production. DNA coding for the B1 domain of peptostreptococcal protein-L with a Y45W mutation, from E0 to G62 (including an additional N-terminal methionine, using the numbering convention of Scalley et al.[25]), was amplified by PCR. The PCR product was inserted between *Nco*I and *Bgl*II restriction endonuclease sites in a pET11d (Novagen) expression plasmid with an ochre stop codon included in the 3′ PCR primer. The integrity of the construct was verified by DNA sequencing. Freshly transformed *Escherichia coli* BL21 DE3 cells were innoculated into 2 L of 50% ^2H_2O M9 minimal medium with $^{15}NH_4Cl$ and ^{13}C-glucose as the sole sources of nitrogen and carbon and grown at 37 °C with aeration. Protein expression was induced at an OD_{600} of 0.7 with the addition of 200 mg/L IPTG and allowed to continue for 4 h. Cells were harvested by centrifugation, and lysis was achieved by sonication. Lysate was heated to 80 °C for 5 min and stirred at 20 °C for 30 min. The aggregate of denatured nonthermostable proteins was removed by centrifugation. The supernatant was applied to an S-300 Amersham Pharmacia gel filtration column, and the appropriate fractions were loaded on a hand-poured Amersham Pharmacia SP-Sepharose column in 20 mM sodium citrate pH 3.5. The protein was eluted with a 0-to-2 M NaCl gradient and was free from contaminants, as established by overloaded SDS−PAGE. Protein concentration was determined by absorbance at 280 nm using a theoretical extinction coefficient predicted on the basis of the primary sequence.[27]

Data Acquisition and Processing. NMR experiments were performed on 0.5 mL, 1.8 mM protein samples at 33 °C using a 600 MHz Varian Inova spectrometer. In the absence of aligning media, sample conditions were 50 mM Na_3PO_4 pH 6.0, 0.05% NaN_3, and 10% ^2H_2O. In a second sample, conditions were identical except for the addition of 19 mg/mL Pf1 bacteriophage.[28] A third sample contained 5% (w/v) 1,2-dimyristoyl-*sn*-glycero-3-phosphocholine/1,2-dihexanoyl-*sn*-glycero-3-phosphocholine bicelles prepared as described previously[29] with 50 mM Na_3PO_4 pH 6.0, 0.01% NaN_3, and 10% ^2H_2O.

$^{13}C^\beta-^1H^\beta$ couplings were obtained from sets comprised of 12 constant-time $^{13}C-^1H$ correlation spectra[30,31] recorded with spectral widths of 9000.9 and 3600.0 Hz, with 576 and 78 complex points in the direct and indirect dimensions, respectively. Mirror-image linear prediction[32] was applied to the ^{13}C dimension of each data set, and both dimensions were apodized with shifted sine-bell window functions, zero-filled to 2048 × 512 complex points, and Fourier transformed using the NMRPipe/NMRDraw suite of programs.[33] Peak volumes were fit using nlinLS software.[33] The $^{13}C^\beta-^1H^\beta$ couplings were allowed to evolve for a period of $2\tau_c - 2\tau_b$ (see Figure 1) set to [−0.01, 1.89, 3.69, 5.59, 7.39, 9.29, 11.09, 12.99, 14.79, 16.69, 18.49, 20.39] ms.

$^{13}C^\alpha-^1H^\alpha$, $^{13}C^\alpha-^{13}C^\beta$, and $^{13}C^\alpha-^{13}C'$ couplings were obtained from sets of 16 HNCO[34]-based $^{15}N-^1H$ correlation spectra (see Supporting Information for pulse schemes and details) with spectral widths of 9000.9, 1338.0 Hz and 576, 80 complex points in the direct and indirect dimensions, respectively. Shifted sine bell apodization was used in both dimensions, followed by zero-filling to 2048 × 256 points and Fourier transformation. Peak intensities were extracted using seriesTab software.[33] Couplings were allowed to evolve for durations of [1.00, 1.78, 3.58, 5.36, 7.14, 8.92, 10.72, 12.50, 14.28, 16.06, 17.86, 19.64, 21.42, 23.20, 25.00, 26.80], [0.50, 3.73, 6.97, 10.23, 13.47, 16.73, 19.97, 23.23, 26.47, 29.73, 32.97, 36.23, 39.47, 42.73, 45.97, 49.23], and [0.10, 2.62, 5.26, 7.88, 10.50, 13.12, 15.78, 18.38, 21.00, 23.62, 26.26, 28.88, 31.50, 34.12, 36.76, 39.38] ms in $^{13}C^\alpha-^1H^\alpha$, $^{13}C^\alpha-^{13}C^\beta$, and $^{13}C^\alpha-^{13}C'$ experiments, respectively.

Data Analysis. Effective $^{13}C^\beta-^1H^\beta$ coupling values, J' (where J' is the sum of scalar and dipolar contributions in the case of aligned protein[35,36] or simply equal to the scalar coupling when measurements are performed in isotropic solution), were extracted from the time dependence of cross-peak intensities (see below) using nonlinear least-squares fitting of a time modulation function,

$$I(t) = [c_1 \cos(\pi J' t) + c_2] \exp\{-(c_3 t)^2\} \quad (1)$$

where $I(t)$ is the intensity of a cross-peak obtained with coupling delay t. The coefficients c_1, c_2, and c_3 are fit simultaneously with J' and account for overall scaling of the data, incomplete ^1H inversion during the constant time coupling evolution period, and multiple long-range $^{13}C-^1H$ couplings,[37] respectively. In practice, the values of c_2 were less than 10^{-3} (with c_1 normalized to 1). All minimizations were performed using the simplex algorithm supplied with the MATLAB software package. Values of $^1D_{C\beta-H\beta^{2,3}}$ and ($^1D_{C\beta-H\beta^2} + {}^1D_{C\beta-H\beta^3}$) dipolar

(22) Case, D. A.; Scheurer, C.; Bruschweiler, R. *J. Am. Chem. Soc.* **2000**, *122*, 10390−10397.
(23) Schmidt J. M.; Blumel M.; Lohr F.; H., R. *J. Biomol. NMR* **1999**, *14*, 1−12.
(24) Tolman, J. R.; Flanagan, J. M.; Kennedy, M. A.; Prestegard, J. H. *Nat. Struct. Biol.* **1997**, *4*, 292−297.
(25) Scalley, M. L.; Yi, Q.; Gu, H.; McCormack, A.; Yates, J. R.; Baker, D. *Biochemistry* **1997**, *36*, 3373−3382.
(26) Wikström, M.; Sjobring, U.; Drakenberg, T.; Forsen, S.; Bjorck, L. *J. Mol. Biol.* **1995**, *250*, 128−133.
(27) Pace, C. N.; Vajdos, F.; Fee, L.; Grimsley, G.; Gray, T. *Protein Sci* **1995**, *4*, 2411−2423.
(28) Hansen, M. R.; Mueller, L.; Pardi, A. *Nat. Struct. Biol.* **1998**, *5*, 1065−1074.
(29) Ottiger, M.; Bax, A. *J. Biomol. NMR* **1999**, *13*, 187−191.
(30) Vuister, G. W.; Bax, A. *J. Magn. Reson.* **1992**, *98*, 428−435.
(31) Santoro, J.; King, G. C. *J. Magn. Reson.* **1992**, *97*, 202−207.
(32) Zhu, G.; Bax, A. *J. Magn. Reson.* **1990**, *90*, 405−410.
(33) Delaglio, F.; Grzesiek, S.; Vuister, G. W.; Zhu, G.; Pfeifer, J.; Bax, A. *J. Biomol. NMR* **1995**, *6*, 277−293.
(34) Kay, L. E.; Ikura, M.; Tschudin, R.; Bax, A. *J. Magn. Reson.* **1990**, *89*, 496−514.
(35) Tolman, J. R.; Flanagan, J. M.; Kennedy, M. A.; Prestegard, J. H. *Proc. Natl. Acad. Sci. U.S.A.* **1995**, *92*, 9279−9283.
(36) Tjandra, N.; Bax, A. *Science* **1997**, *278*, 1111−1114.
(37) Ottiger, M.; Delaglio, F.; Marquardt, J. L.; Tjandra, N.; Bax, A. *J. Magn. Reson.* **1998**, *134*, 365−369.

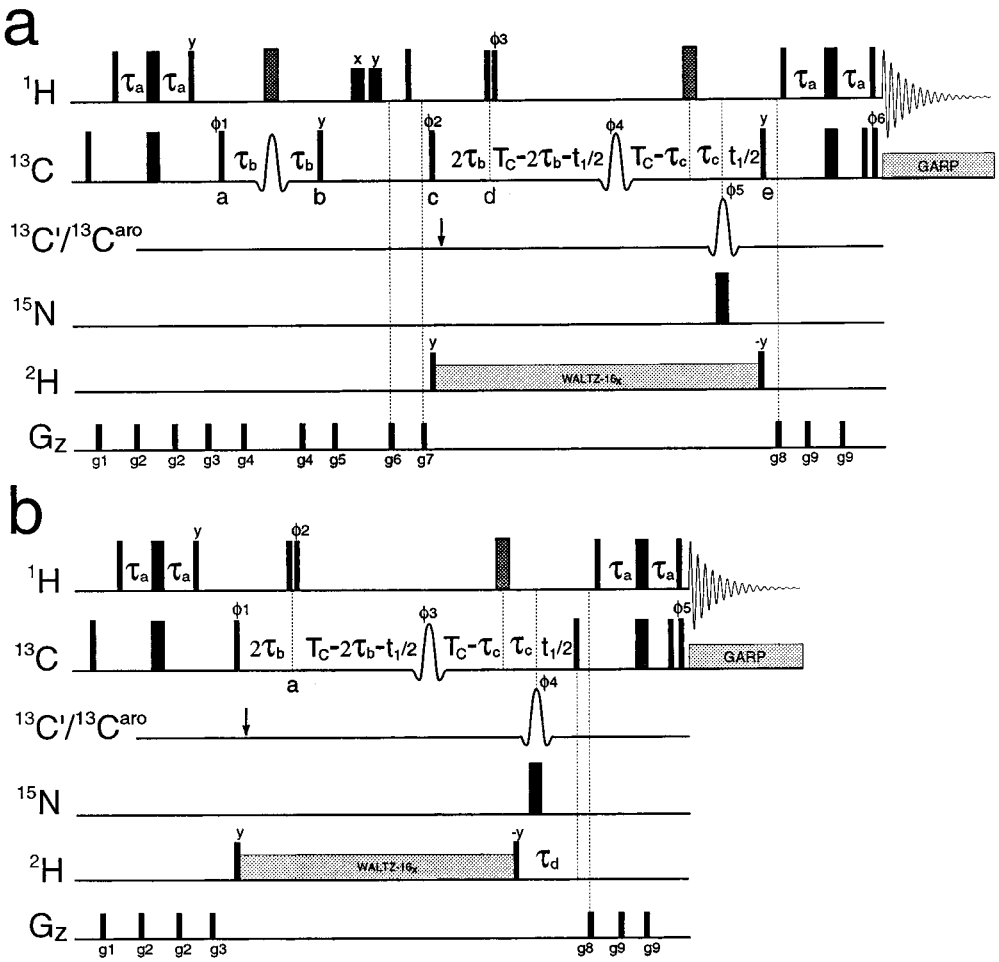

Figure 1. Pulse schemes used to measure (a) one-bond $^{13}C-^{1}H$ dipolar couplings with selection of CHD methylene groups and (b) the sum of one-bond $^{13}C-^{1}H$ dipolar couplings in CH_2 groups. All narrow (wide) pulses are applied with a flip angle of 90° (180°) unless otherwise indicated. The ^{1}H, ^{13}C, ^{15}N, and ^{2}H carriers are positioned at 4.73 (water), 43, 119, and 3 ppm, respectively. All ^{1}H pulses are applied with a field strength of 31 kHz, with the exception of the *x* (6 ms) and *y* (5 ms) purge pulses after point b, which use a 7 kHz field. The shaded ^{1}H 180° pulses are of the composite variety.[55] All ^{13}C rectangular pulses make use of an 18 kHz field; the shaped ^{13}C pulses have a REBURP profile[56] (400 μs, 180°), while the $^{13}C'/^{13}C^{aro}$ pulses are centered at 150 ppm (310 μs, G3 shape[57]) and simultaneously invert carbonyl and aromatic carbons. The arrow indicates the position of the Bloch−Siegert compensation pulse[30] (310 μs, G3). ^{13}C decoupling during acquisition is achieved with a 3.3 kHz GARP-1 field.[58] The ^{2}H 90° pulses which flank the 0.65 kHz ^{2}H decoupling train are applied at a field of 2 kHz. The delays used are $\tau_a = 1.70$ ms; $\tau_b = 1.87$ ms; $T_C = 14.7$ ms; τ_c is varied between experiments (see Materials and Methods); $\tau_d = 11$ ms. Quadrature detection in F_1 is achieved by States-TPPI[59] of $\phi 2$ (a) and $\phi 1$ (b). The phase cycle employed is $\phi 1 = x,-x$; $\phi 2 = x$; $\phi 3 = x,-x$; $\phi 4 = 2(x),2(y),2(-x),2(-y)$; $\phi 5 = 4(x),4(-x)$; $\phi 6 = x,-x$; rec $= 2(x),2(-x)$ in (a), while in (b) $\phi 1 = 8(x),8(-x)$; $\phi 2 = x,-x$; $\phi 3 = 2(x),2(y),2(-x),2(-y)$; $\phi 4 = 4(x),4(-x)$; $\phi 5 = x,-x$; rec $= 2(x,-x,-x,x),2(-x,x,x,-x)$. The gradients used are $g1 = 0.5$ ms, 5 G/cm; $g2 = 0.2$ ms, 6 G/cm; $g3 = 1.5$ ms, 15 G/cm; $g4 = 0.2$ ms, 5 G/cm; $g5 = 0.5$ ms, 6 G/cm; $g6 = 1.0$ ms, 15 G/cm; $g7 = 2.0$ ms, 10 G/cm; $g8 = 0.6$ ms, 10 G/cm; $g9 = 0.2$ ms, 2 G/cm. The intensity of gradient $g8$ is inverted with $\phi 3$ (a) and $\phi 2$ (b) to minimize the residual water signal.[4]

couplings were obtained from the CHD and CH_2 selective experiments, respectively, by subtracting $J'_{isotropic}$ from $J'_{aligned}$.

Backbone $^{13}C^{\alpha}-^{1}H^{\alpha}$, $^{13}C^{\alpha}-^{13}C^{\beta}$, and $^{13}C^{\alpha}-^{13}C'$ dipolar couplings were also measured, using an approach in which cross-peak intensities are modulated by the desired coupling, as described below. The time modulation function for the $^{13}C^{\alpha}-^{1}H^{\alpha}$ experiment was identical to that described above for $^{13}C^{\beta}-^{1}H^{\beta}$ couplings (eq 1), with the parameter c_2 additionally accounting for incomplete suppression of magnetization from $^{13}C^{\alpha}-^{2}H^{\alpha}$ systems. Since the approach used to purge magnetization from $^{13}C^{\alpha}-^{2}H^{\alpha}$ spin pairs does not eliminate signal from the middle line of the ^{13}C triplet (see Supporting Information, supplemental figure c), the values of c_2 in the fits were somewhat larger than those obtained in the $^{13}C^{\beta}-^{1}H^{\beta}$ experiments. The function

$$I(t) = [c_1 \cos(\pi J' t) + c_2] \exp\{-c_3 t\} \qquad (2)$$

was used to fit peak intensities in the $^{13}C^{\alpha}-^{13}C^{\beta}$ and $^{13}C^{\alpha}-^{13}C'$ coupling experiments. In this case, the coefficient c_3 accounts for the transverse relaxation of $^{13}C'$ and $^{13}C^{\alpha}$ nuclei in the $^{13}C^{\alpha}-^{13}C'$ and $^{13}C^{\alpha}-^{13}C^{\beta}$ experiments, respectively, during the non-constant-time periods when evolution due to couplings occurs.

The measured backbone dipolar couplings, $^{1}D_{C\alpha-H\alpha}$, $^{1}D_{C\alpha-C\beta}$, and $^{1}D_{C\alpha-C'}$, were used in concert with a recently determined crystal structure of the protein-L B1 domain[38] (in which three copies of the molecule are present in the asymmetric unit, PDB accession code 1HZ6) to obtain alignment frame parameters A_a and R and the Euler angles, Ω, describing the orientation of the alignment frame in the PDB frame.[36] In the analyses described below, the second molecule in the asymmetric unit was used since the best correlation between NMR measured couplings and predicted values was obtained with this structure. $^{1}D_{C\beta-H\beta}$[2,3] dipolar couplings were subsequently calculated using the relationship[36]

$$^{1}D(\vec{\nu}) = -\frac{\gamma_H \gamma_C h A_a}{4\pi^2 r^3_{C\beta-H\beta}}(3\nu_z^2 - 1 + {}^3/_2 R(\nu_x^2 - \nu_y^2)) \qquad (3)$$

where $\vec{\nu} = (\nu_x, \nu_y, \nu_z)$ is a unit vector parallel to the $C^{\beta}-H^{\beta}$ bond as

(38) O'Neill, J. W.; Kim, D. E.; Baker, D.; Zhang, K. Y. J. *Acta Crystallogr.* **2001**, *D57*, 480−487.

defined in the molecular alignment frame, γ_H and γ_C are the gyromagnetic ratios of ^{1}H and ^{13}C nuclei, h is Planck's constant, and $r_{C\beta-H\beta}$ is the effective separation of the two nuclei, assumed to be equal to $r_{C\alpha-H\alpha} = 1.117$ Å.[39] Values of $^1D_{C\alpha-H\alpha}$, $^1D_{C\alpha-C\beta}$, and $^1D_{C\alpha-C'}$ were calculated similarly using $r_{C\alpha-C\beta} = 1.517$ Å[40] and $r_{C\alpha-C'} = 1.526$ Å.[39]

$^1D_{C\beta-H\beta^{2,3}}$ values were calculated as a function of the dihedral angle χ_1, making use of the fact that the C′−C$^\alpha$ and the C$^\beta$−H$^{\beta2}$ bond vectors are parallel (so, too, are the H$^\alpha$−C$^\alpha$ and C$^\beta$−H$^{\beta3}$ bond vectors) in the case of ideal tetrahedral geometry when $\chi_1 = 180°$. The orientations of the two C$^\beta$−H$^\beta$ bond vectors may then be calculated for any value of χ_1 using the following relationships:

$$\vec{\nu}_{C\beta-H\beta2}(\chi_1) = R_{C\alpha-C\beta}(\chi_1 + 180°)\cdot\vec{\nu}_{C'-C\alpha} \quad (4a)$$

and

$$\vec{\nu}_{C\beta-H\beta3}(\chi_1) = R_{C\alpha-C\beta}(\chi_1 + 180°)\cdot\vec{\nu}_{H\alpha-C\alpha} \quad (4b)$$

where $R_{C\alpha-C\beta}(x)$ represents a right-handed rotation of x degrees about the C$^\alpha$−C$^\beta$ bond and $\vec{\nu}_{A-B}$ is a unit vector parallel to the A−B internuclear vector.

As described in the Results section, three motional models were used to fit the C$^\beta$−H$^\beta$ dipolar couplings measured in two alignment media: a static model (A), a model in which the dynamics in a given rotamer well are described in terms of a Gaussian distribution of χ_1 values (B), and a three-site jump model (C). Optimization of parameters in models A and C was accomplished by using the MATLAB simplex algorithm. Minimization of the target function for model B was performed by an initial grid search over mean dihedral angles, $\bar{\chi}_1$, and standard deviations, ρ, in 0.5° and 2° increments, respectively, followed by a search over the global minimum in 0.1° increments in both dimensions. A maximum value of $\rho = 30°$ was employed.

χ_1 values in model C were selected at random for each canonical rotamer and residue type from Gaussian distributions defined by the mean and standard deviations of χ_1 angles from a database of high-resolution crystal structures reported by Ponder and Richards.[41] In the cases that χ_1 has different distributions depending on the values of χ_2 or χ_3, distributions were selected randomly with a frequency proportional to their occurrence in the database.

The statistical significance of one model over another has been evaluated using F-test statistics, as described previously.[42,43] Given two models with $\nu_1 > \nu_2$ degrees of freedom (number of measurements minus number of parameters) and with residual errors $\chi_1^2 > \chi_2^2$, the quantity

$$F = \frac{\chi_1^2 - \chi_2^2}{(\nu_1 - \nu_2)(\chi_2^2/\nu_2)} \quad (5)$$

can be used to assess the validity of adding $(\nu_1 - \nu_2)$ fitting parameters by calculating the probability $p(F,(\nu_1 - \nu_2),\nu_2)$ that a reduction in χ^2 as large as or larger than the one observed could occur simply by chance.[44] Note that model A uses a single fitted parameter with two such parameters for models B and C. Since four experimental measurements are available for β-methylene-containing residues ($^1D_{C\beta-H\beta^2}$ and $^1D_{C\beta-H\beta^3}$ derived from both phage and bicelle aligned samples), $\nu_2 = 2$ and $(\nu_1 - \nu_2) = 1$ in a calculation of the statistical significance of either model B or C relative to A.

The program MOLMOL[45] was used to place protons in the crystal structure of protein-L. This software was also used to calculate solvent accessibility on a per-atom basis with a 1.4 Å probe. Accessibility at the C$^\beta$ position was defined as the solvent accessible area of the C$^\beta$H$^\beta{}_2$ unit normalized by the total area of the methylene moiety. Hydrogen bonds were identified only if the distance between the hydrogen and the heavy atom acceptor group was less than 2.4 Å with a maximum deviation from linearity of 35° in the acceptor−H−donor angle.

Results

Measurement of ^{13}C$^\beta$−^{1}H$^\beta$ Dipolar Couplings. ^{13}C$^\beta$−^{1}H$^\beta$ dipolar couplings are obtained from a series of constant-time ^{13}C−^{1}H correlation spectra[30,31] where the intensity of each cross-peak is modulated by evolution due to either $^1J_{C\beta-H\beta^i} + {}^1D_{C\beta-H\beta^i}$ $\{i = 2,3\}$ (Figure 1a) or $^1J_{C\beta-H\beta^2} + {}^1D_{C\beta-H\beta^2} + {}^1J_{C\beta-H\beta^3} + {}^1D_{C\beta-H\beta^3}$ (Figure 1b) couplings, where J and D are scalar and dipolar couplings, respectively. In these experiments, a uniformly ^{13}C, ∼50% fractionally deuterated protein is employed in which either ^{13}CHD methylene groups (Figure 1a) or ^{13}CH$_2$ methylene groups (Figure 1b) are selected. In the scheme of Figure 1a, magnetization is transferred from ^{1}H to ^{13}C, with the desired signal of the form $2C_YI_Z$ at point a, where C_Y and I_Z are the y and z components of ^{13}C and ^{1}H magnetization, respectively. During the interval extending from a to b, of duration $2\tau_b = 1/(2\,{}^1J_{C\beta-H\beta})$, the difference in the way magnetization derived from CHD and CH$_2$ moieties evolves under ^{13}C−^{1}H scalar coupling is exploited so that signal from CHD methylenes is selected while magnetization from CH$_2$ moieties is suppressed. Focusing on magnetization of the form $2C_YI^i{}_Z$ $\{i = 2, 3\}$ at point a in the sequence and neglecting relaxation, immediately after the application of the ^{13}C 90°_y pulse at point b, the term of interest (from CHD) is given by

$$C_Z \sin\{\pi(^1J_{C\beta-H\beta^i} + {}^1D_{C\beta-H\beta^i})2\tau_b\} \quad (6)$$

while undesired terms of the form

$$C_Z \sin\{\pi(^1J_{C\beta-H\beta^i} + {}^1D_{C\beta-H\beta^i})2\tau_b\} \cos\{\pi(^1J_{C\beta-H\beta^j} + {}^1D_{C\beta-H\beta^j})2\tau_b\} + 4C_ZI_Z^2I_Z^3 \sin\{\pi(^1J_{C\beta-H\beta^j} + {}^1D_{C\beta-H\beta^j})2\tau_b\} \cos\{\pi(^1J_{C\beta-H\beta^i} + {}^1D_{C\beta-H\beta^i})2\tau_b\} \quad (7)$$

with $\{i = 2, j = 3\}$ or $\{i = 3, j = 2\}$ arise from CH$_2$ groups. In the case where $^1D_{C\beta-H\beta} \approx 0$ (for example, in the absence of alignment), the terms in eq 7 can be efficiently suppressed since one-bond ^{13}C$^\beta$−^{1}H$^\beta$ scalar couplings are quite uniform in proteins. However, in the case of significant variation in $^1J_{C\beta-H\beta} + {}^1D_{C\beta-H\beta}$ values, additional purging is often necessary. In this regard, the pulses between points b and c decrease contributions that originate from the term proportional to $4C_ZI_Z^2I_Z^3$ (eq 7). In addition, these pulses also reduce the residual water signal considerably, as described previously.[46] A second purge element is inserted at point d in the scheme, where the application of a ^{1}H $90_x90_{\phi3}$ pulse-pair with $\phi3$ and the phase of the receiver inverted together also serves to suppress signal from CH$_2$ groups.[4] During the interval extending from c to e, ^{13}C chemical shift is recorded during t_1, and at point e the signal of interest is modulated according to ($\phi2 = x$)

$$\cos(\omega_C t_1) \sin^2\{\pi(^1J_{C\beta-H\beta^i} + {}^1D_{C\beta-H\beta^i})2\tau_b\} \cos\{\pi(^1J_{C\beta-H\beta^i} + {}^1D_{C\beta-H\beta^i})(2\tau_c - 2\tau_b)\} \quad (8)$$

Magnetization is subsequently transferred back to protons for observation, so that for each ^{13}C$^\beta$−^{1}H$^{\beta,i}$ $\{i = 2, 3\}$ pair a correlation is obtained with an intensity proportional to the expression given by eq 8. Thus, by recording a series of spectra

(39) Ottiger, M.; Bax, A. *J. Am. Chem. Soc.* **1998**, *120*, 12334−12341.
(40) Engh, R. A.; Huber, R. *Acta Crystallogr.* **1991**, *A47*, 392−400.
(41) Ponder, J. W.; Richards, F. M. *J. Mol. Biol.* **1987**, *193*, 775−791.
(42) Tjandra, N.; Feller, S. E.; Pastor, R. W.; Bax, A. *J. Am. Chem. Soc.* **1995**, *117*, 12562−12566.
(43) Gagne, S. M.; Tsuda, S.; Spyracopoulos, L.; Kay, L. E.; Sykes, B. D. *J. Mol. Biol.* **1998**, *278*, 667−686.
(44) Bevington, P. R.; Robinson, D. K. *Data Reduction and Error Analysis for the Physical Sciences*; WCB/McGraw-Hill: New York, 1992.
(45) Koradi, R.; Billeter, M.; Wüthrich, K. *J. Mol. Graphics* **1996**, *14*, 51−55.
(46) Kay, L. E. *J. Am. Chem. Soc.* **1993**, *115*, 2055−2057.

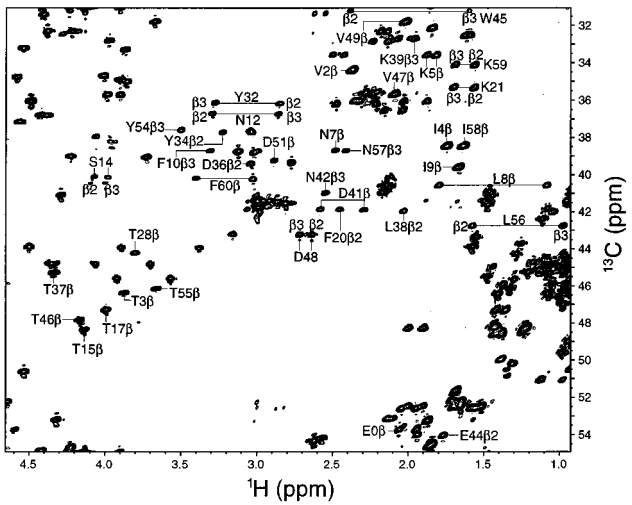

Figure 2. $^{13}C-^{1}H$ correlation map of the B1 domain of protein-L recorded at 600 MHz (^{1}H frequency) using the pulse scheme of Figure 1a, with the time for evolution of $^{13}C^{\beta}-^{1}H^{\beta}$ couplings, $(2\tau_c - 2\tau_b)$, set to zero. Only peaks used to obtain $^{1}D_{C\beta-H\beta}$ are labeled (according to the numbering convention of Scalley et al.[25]). Where only a single peak of a methylene group is resolved, dipolar couplings for the other $^{13}C-^{1}H$ spin pair were obtained indirectly, as described in the text. Stereoassignments obtained exclusively from dipolar coupling analyses are also included.

as a function of τ_c and fitting cross-peak intensities to eq 8, $(^{1}J_{C\beta-H\beta^i} + {}^{1}D_{C\beta-H\beta^i})$ is readily extracted and the dipolar coupling values are obtained by recording spectra with and without alignment.

Figure 1b shows the pulse scheme for measuring $(^{1}D_{C\beta-H\beta^2} + {}^{1}D_{C\beta-H\beta^3})$ in ^{13}C-labeled, fractionally deuterated samples. This experiment is similar to one published recently by Bax and coworkers[37] with the exception that, in the present case, care must be taken to ensure that only signal from the CH_2 isotopomer is selected. This is accomplished by the ^{1}H 90_x $90_{\phi 2}$ pulse pair at point *a* in the pulse scheme, which selects for coherences of the form $2C_YI_Z$. Note that magnetization arising from CHD groups is largely in-phase at this point. Further suppression of signals from CHD moieties is achieved by allowing evolution from $^{13}C-^{2}H$ couplings to proceed for a period $\tau_d = 1/(4\,J_{CD})$, effectively eliminating the outer components of the triplet associated with the CHD group.[47] In this case, cross-peak intensities in the resultant 2D $^{1}H-^{13}C$ correlation map are modulated according to

$$\cos\{\pi(^{1}J_{C\beta-H\beta^2} + {}^{1}D_{C\beta-H\beta^2} + {}^{1}J_{C\beta-H\beta^3} + {}^{1}D_{C\beta-H\beta^3})(2\tau_c - 2\tau_b)\} \quad (9)$$

and $^{1}D_{C\beta-H\beta^2} + {}^{1}D_{C\beta-H\beta^3}$ is extracted from measurements recorded with and without alignment, as described previously. In both experiments, excellent suppression of signal corresponding to the unwanted isotopomer is achieved.

Figure 2 illustrates a $^{1}H-^{13}C$ correlation map of protein-L recorded with the pulse scheme of Figure 1a on an unaligned sample with the time for evolution of $^{13}C^{\beta}-^{1}H^{\beta}$ couplings, $(2\tau_c - 2\tau_b)$, set to zero. The β-methylene groups in the protein are labeled, and in cases where stereospecific assignments have been obtained (using the methodology described in the present paper, see below), they have been included. For a number of residues such as N57, only one of the two expected correlations is resolved in this spectrum due to overlap. In these cases, it is still possible to obtain the value of the dipolar coupling associated with the spin pair that gives rise to the unresolved correlation since individual dipolar couplings, $^{1}D_{C\beta-H\beta^{2,3}}$ are obtained from the experiment of Figure 1a, while sums of couplings, $^{1}D_{C\beta-H\beta^2} + {}^{1}D_{C\beta-H\beta^3}$, are measured using the scheme of Figure 1b.

There are 49 $^{13}C^{\beta}$ spin systems available for analysis in protein-L, not counting the N-terminal methionine or the alanine residues in the protein. Five of these have degenerate H^{β} chemical shifts, while for two of the residues the $^{13}C^{\beta}$ carbon is strongly coupled to directly bonded ^{13}C spins. Both $^{13}C^{\beta}-^{1}H^{\beta 2,3}$ correlations are completely overlapped by other peaks in three instances and one threonine H^{β} resonance is obscured by residual signal from $^{1}H_2O$. Of the 38 remaining residues, three were not used in the study of dynamics because backbone dipolar couplings could not be obtained due to spectral overlap (see below). Finally, the second residue from the N-terminus was discarded because the orientation of its backbone ($^{1}H^{\alpha}$, $^{13}C^{\alpha}$, $^{13}C^{\beta}$, $^{13}C'$) could not be well fit using dipolar coupling data recorded on samples aligned in Pf1 phage and bicelles (see below), likely due to the presence of significant backbone dynamics.

Figure 3 illustrates the time dependence of cross-peak intensities for residue D48 in protein-L obtained from CHD (Figure 3a) and CH_2 (Figure 3b) selective experiments, respectively. In this particular example, the protein is aligned with Pf1 phage, and the two D48 $^{13}C^{\beta}-^{1}H^{\beta}$ dipolar couplings differ by more than 20 Hz (Figure 3a). In Figure 3b, the intensity profile of each $^{13}C^{\beta}-^{1}H^{\beta}$ correlation reports the sum of scalar and dipolar couplings for both $^{13}C^{\beta}-^{1}H^{\beta}$ spin pairs so that the same modulation should be observed, irrespective of which cross-peak is examined; sums of couplings obtained from the two cross-peaks (solid and dashed lines in Figure 3b) differ by less than 0.1 Hz. The high quality of the data is further established by the small difference between the sum of the individual $^{13}C^{\beta}-^{1}H^{\beta}$ dipolar couplings obtained for a given residue (CHD selection) and the sum of couplings extracted from measurements that select for CH_2 methylenes (rmsd of 1.1 Hz for the 12 residues with two resolved β protons). Since a range of greater than 65 Hz in sums of dipolar couplings is observed, this amounts to a relative error of less than 2%. The pairwise rmsd of $(^{1}J + {}^{1}D)_{C\beta-H\beta^i}$ $\{i = 2,3\}$ values in repeat experiments, utilizing the CH_2-selective experiment when necessitated by cross-peak overlap, is 0.32 Hz (Figure 3c).

Comparison with an X-ray Crystal Structure. In addition to $^{1}D_{C\beta-H\beta}$ measurements, backbone $^{1}D_{C\alpha-H\alpha}$, $^{1}D_{C\alpha-C\beta}$, and $^{1}D_{C\alpha-C'}$ values were obtained using pulse sequences described in the Supporting Information. Alignment parameters, A_a and R, and Euler angles, Ω, were subsequently calculated for both phage and bicelle aligning media using these couplings and a high-resolution crystal structure of the B1 domain of protein-L,[38] as described in the Materials and Methods section. Significantly different alignment frames were obtained for the two aligning media, with A_a and R values of -7.1×10^{-4}, 0.57 and -1.3×10^{-3}, 0.47 for phage and bicelles, respectively, and with the *z*-axes of the alignment frames differing by 80°. That the alignment frames are very different is also established by the fact that the correlation between experimental couplings measured in the two aligning media is very poor. For example, the pairwise rmsd between $^{13}C^{\alpha}-^{1}H^{\alpha}$ couplings obtained from the two media is 35.7 Hz, with a linear correlation coefficient of -0.32.

Figure 3d illustrates the correlation between experimental and calculated $^{1}D_{C\beta-H\beta^{2,3}}$ values, with the predicted values based

(47) Gardner, K. H.; Rosen, M. K.; Kay, L. E. *Biochemistry* **1997**, *36*, 1389−1401.

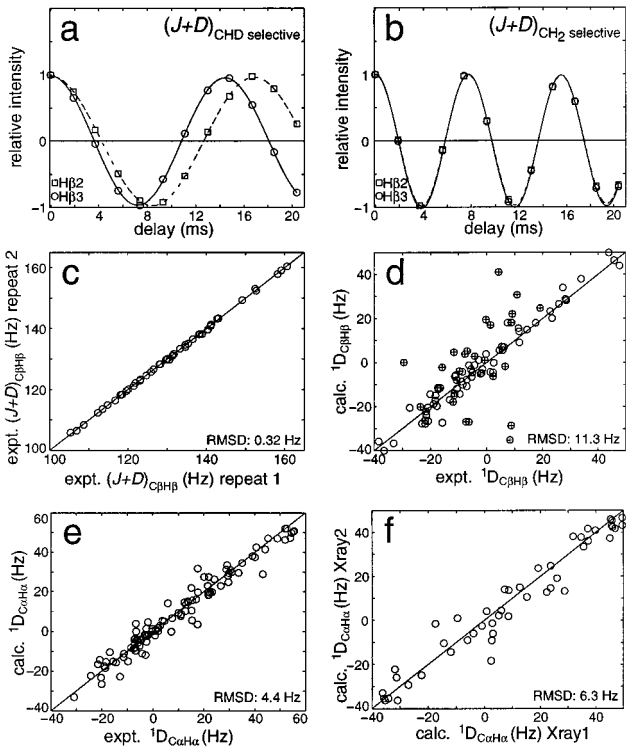

Figure 3. Time dependence of cross-peak intensities for residue D48 in protein-L oriented with Pf1 phage (~19 mg/mL) obtained from CHD (a)- and CH_2 (b)-selective experiments. In (a) the intensity profile of each correlation (intensities of $C^{\beta}-H^{\beta 2}$ and $C^{\beta}-H^{\beta 3}$ cross-peaks are indicated with squares and circles, respectively) yields the individual $^{13}C-^{1}H$ dipolar couplings, while in (b) each correlation evolves with the sum of scalar and dipolar couplings from both $^{13}C^{\beta}-^{1}H^{\beta}$ methylene spin pairs. (c) Correlation of $(^{1}J_{C\beta-H\beta} + {}^{1}D_{C\beta-H\beta})$ values, including those indirectly calculated for overlapped peaks, obtained in repeat experiments measured in Pf1 phage. (d) Correlation of experimental methylene $^{1}D_{C\beta-H\beta}$[2,3] values (phage and bicelle data included) with those calculated using molecule two of the three in the asymmetric unit.[38] Data from residues best fit by a rotamer-jump model are indicated with ⊕. For this plot, stereoassignments were selected to maximize agreement with the crystal structure. (e) Correlation of $^{1}D_{C\alpha-H\alpha}$ values obtained experimentally and predicted as described above (phage and bicelle data included). (f) Correlation of predicted $^{1}D_{C\alpha-H\alpha}$ values obtained from molecules one and two of the three X-ray copies, first aligned to maximize collinearity of corresponding $C^{\alpha}-H^{\alpha}$, $C^{\alpha}-C^{\beta}$, and $C^{\alpha}-C'$ bond vectors. Parameters A_a, R, and Ω obtained for the bicelle-oriented sample were used in the calculation of $^{1}D_{C\alpha-H\alpha}$ values. Extreme outlier points corresponding to E0, I9, and A11 are omitted from the plot.

on the orientations of $C^{\beta}-H^{\beta}$ internuclear vectors from the crystal structure. Clearly the correlation is poor, with discrepancies arising partly from motion about the χ_1 dihedral angle, since the worst agreement is obtained for residues which are subsequently shown to adopt multiple rotameric states (indicated by ⊕, see below). Discarding these points reduces the pairwise rmsd to 4.3 Hz, which is still an order of magnitude greater than the intrinsic experimental uncertainty (0.32 Hz). In summary, fits of the experimental data using a single rigid X-ray structure are unsatisfactory.

In addition to dynamics, relatively small differences in structure between the crystalline and solution states of the protein could cause further disagreement between predicted and observed dipolar couplings. In the case of $C^{\beta}-H^{\beta}$ bond vectors, structural variations may arise due to differences in the χ_1 dihedral angle and local rearrangements of the backbone, including the $C^{\alpha}-C^{\beta}$ bond vector. To investigate the magnitude of the second contribution, we compared predicted and experimental $^{1}D_{C\alpha-H\alpha}$ values (Figure 3e), and the rmsd obtained, 4.4 Hz, is again much larger than the precision of the measurements (0.36 Hz). The crystal structure of protein-L contains three molecules in the asymmetric unit, thus providing a useful estimate of the structural uncertainty. The mean pairwise rmsd of the backbone (N, C^{α}, C′) atoms is 0.65 Å (averaged over the three molecules), and Figure 3f illustrates the rather poor agreement between $^{1}D_{C\alpha-H\alpha}$ values calculated using the first and second molecules in the asymmetric unit and values for A_a, R, and Ω determined previously. It is clear that the structural uncertainty at the level of the backbone atoms is sufficient to explain the differences between calculated and experimental $^{1}D_{C\alpha-H\alpha}$ values and must be accounted for in a quantitative analysis of $^{1}D_{C\beta-H\beta}$ values in terms of χ_1 torsion angle dynamics.

Reorienting Backbone Fragments. To address the uncertainty associated with the orientations of the backbone fragments, we have developed the following approach which makes use of the backbone dipolar couplings to reorient each fragment ($^{1}H^{\alpha}$, $^{13}C^{\alpha}$, $^{13}C^{\beta}$, and $^{13}C'$ atoms). The algorithm that we employ is essentially a rigid-body minimization intended to refine the orientations of the individual backbone units, similar to the approach developed by Mueller et al.[48] With the six measured dipolar coupling restraints per backbone unit ($^{1}D_{C\alpha-H\alpha}$, $^{1}D_{C\alpha-C\beta}$, and $^{1}D_{C\alpha-C'}$ from phage and bicelle aligned samples), it is possible to confidently obtain the three parameters (θ,φ,ξ) which describe the rotation of a particular fragment from its orientation in the crystal structure to one which better corresponds to its position in solution. Here, the parameter ξ gives the magnitude of rotation about an axis defined by polar angles θ and φ. The fitting procedure employed is comprised of three steps. In step 1, initial residue fragment orientations are obtained from one of the molecules in the crystal structure. Subsequently, in step 2, dipolar coupling data from bicelle and phage alignment media are analyzed separately to give two sets of alignment frame parameters by minimizing an error function for each data set:

$$\chi^2_{\text{normalized,frame}} = \frac{1}{3N}\sum_{i=1}^{N}\left[\left(\frac{(\Delta^1 D_{(C\alpha-H\alpha)})_i^2}{\sigma^2_{(C\alpha-H\alpha)}}\right) + \left(\frac{(\Delta^1 D_{(C\alpha-C')})_i^2}{\sigma^2_{(C\alpha-C')}}\right) + \left(\frac{(\Delta^1 D_{(C\alpha-C\beta)})_i^2}{\sigma^2_{(C\alpha-C\beta)}}\right)\right] \quad (10)$$

where i is the fragment number, N is the number of fragments, σ is the experimental error estimated as $1/\sqrt{2}$ of the pairwise rmsd obtained in duplicate measurements of the couplings, $\Delta^1 D = {}^{1}D_{\text{experimental}} - {}^{1}D(A_a,R,\Omega)_{\text{calculated}}$. In step 3, individual residues are reoriented independently by combining dipolar coupling data from the two media (six couplings for each residue), using the parameters (A_a, R, Ω) obtained in step 2, and minimizing the target function

$$\chi^2_{\text{fragment}} = \sum_{\substack{i=\text{phage,}\\ \text{bicelle}}}\sum_{\substack{j=\text{H}\alpha,\\ C',C\beta}}\frac{(\Delta^1 D_{i,(C\alpha-j)})^2}{\sigma^2_{(C\alpha-j)}} \quad (11)$$

where $\Delta^1 D = {}^{1}D_{\text{experimental}} - {}^{1}D(\theta,\varphi,\xi)_{\text{calculated}}$. Since differences between the solution structure and the structure used in step 1 may introduce errors in the initial alignment parameter estimates (A_a, R, Ω), steps 2 and 3 are repeated to obtain increasingly consistent alignment frame parameters and fragment orienta-

(48) Mueller, G. A.; Choy, W. Y.; Yang, D.; Forman-Kay, J. D.; Venters, R. A.; Kay, L. E. *J. Mol. Biol.* **2000**, *300*, 197−212.

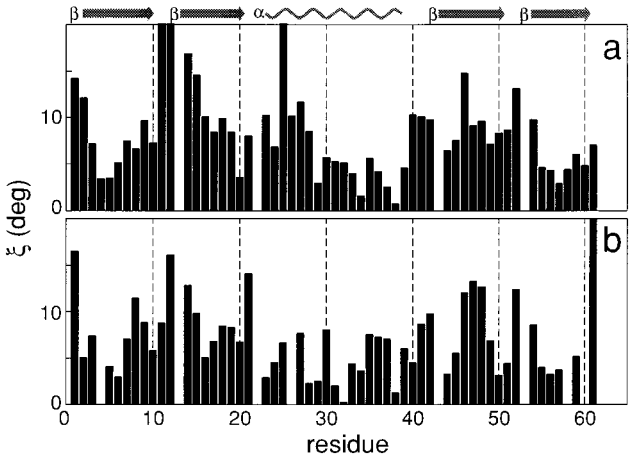

Figure 4. (a) Rotation amplitudes, ξ, about axes with polar angles θ,φ (not reported), which reorient backbone fragments from molecules one to two of the crystal structure and (b) from molecule two to fragments obtained after reorientation using backbone dipolar couplings. Initial and target protein structures are aligned to maximize collinearity of corresponding $C^{\alpha}-H^{\alpha}$, $C^{\alpha}-C^{\beta}$, and $C^{\alpha}-C'$ bond vectors. Rotations (θ,φ,ξ) are subsequently determined which maximize collinearity of the bond vectors of the individual backbone fragments.

tions. The greatest improvement in fit occurs during the first iteration; 10 repetitions are more than sufficient to obtain convergence. The assumption that a single backbone conformation for each residue can explain both phage and bicelle data is supported by the reasonable final χ^2 value (a final χ^2 value, eq 10, of 4 is obtained relative to 70 for the initial value). While principal components of the alignment tensor do not change greatly during this procedure (a 3% increase in R_{bicelle} represents the largest difference), the orientations of the fragments are considerably altered. The magnitude of these changes, however, is well within the structural uncertainty defined by the three molecules of the crystal structure. For example, the rotation which relates the orientations of a given fragment in superimposed molecules one and two from the crystal structure (Figure 4a) is generally of the same magnitude (on average $\xi_{\text{Xtal}} = 8.4°$, $\xi_{\text{dip}} = 7.3°$) as the rotation obtained by fitting to dipolar couplings (Figure 4b).

Fitting of Dynamic Models. To characterize mobility about the χ_1 dihedral angle, the $^{13}C^{\beta}-^{1}H^{\beta}$ dipolar couplings were analyzed in the context of three motional models, with the results summarized in Table 1. It is important to keep in mind that in the analysis of our data we have assumed (i) that the local geometry (bond lengths and angles) of each fragment is correctly described by the X-ray coordinates, (ii) that backbone atoms for each residue have the same dynamics (uncorrelated with side-chain motions), (iii) that the orientation of each fragment in solution can be correctly determined on the basis of the six measured backbone dipolar couplings, and (iv) that the structure of the protein is unchanged in the two alignment media.

Model A. This model assumes that there is no motion about χ_1. Using the alignment parameters and fragment orientations derived above, $^{1}D_{C\beta-H\beta^{2,3}}$ values are predicted as a function of χ_1 (two values for β-methylene-containing residues and one for those with only a single β proton for each alignment medium). The best-fit value of χ_1 is obtained by minimizing a residue-specific function:

$$\chi_A^2 = \sum_{\substack{i=\text{phage,}\\ \text{bicelle}}} \sum_{k=1}^{N} \frac{(^{1}D_{\text{ex}} - {}^{1}D(\chi_1)_{\text{calc}})_{i,k}^2}{2No_i^2} \qquad (12)$$

where $^{1}D(\chi_1)_{\text{calc}}$ is given by eqs 3 and 4, $^{1}D_{\text{ex}}$ is an experimental $^{1}D_{C\beta-H\beta^{2,3}}$ value, k sums over the β protons, σ_i is the experimental error, and N is the number of β protons (1 or 2). For β-methylene-containing residues, optimal values of χ_1 are obtained for both stereoassignments (subsequently referred to as (i) and (ii)) generated by exchanging dipolar coupling data for $H^{\beta 2}$ and $H^{\beta 3}$. Representative plots of χ_A^2 as a function of the χ_1 dihedral angle are shown in Figure 5. In some cases (panels a and b), the experimental dipolar coupling data are sufficient to determine a single stereoassignment and a unique value for χ_1. For 12 residues in protein-L (F10, N12, F20, Y32, Y34, D36, L38, N42, W45, Y54, L56, and N57), the global and next lowest minima are separated by more than an order of magnitude, and the values of χ_1 obtained for these residues are in excellent agreement with the mean values obtained from the crystal structure of the molecule,[38] with a pairwise rmsd of 5.2°. The standard deviations of χ_1 calculated for the same residues in the three molecules of the asymmetric unit are of comparable magnitude, with a mean value of 4.2°. For certain residues, including K5 shown in Figure 5c, no values of χ_1 accommodate the experimental data for either stereoassignment. The dipolar couplings for these residues are significantly better fit by a rotamer-jump model discussed later in the text. A representative plot of χ_A^2 as a function of χ_1 for a residue containing only a single H^{β}, V2, is shown in Figure 5d. For residues V2, T3, I9, V47, V49, and T55 (i.e., excluding residues that are best fit using the χ_1 jump model and T28, whose best-fit value is physically unlikely, see below), the rmsd between dipolar coupling-derived and mean crystallographic χ_1 values is 11°. The increased difference between NMR and X-ray values in this case likely reflects the fact that there are only two dipolar couplings measured for these residues (one from each alignment medium), so that fitted parameters are more susceptible to sources of error such as unaddressed dynamics, misalignment of the backbone fragment, or distorted local geometry.

Model B. In this model, small-amplitude motion within a potential well is assumed to occur. The motion can be described in terms of a Gaussian distribution of χ_1 values centered about a mean value $\bar{\chi}_1$, with a standard deviation ρ, where the probability of a given χ_1 value is expressed by

$$p_{\bar{\chi}_1,\rho}(\chi_1) = \frac{\exp\{-(\bar{\chi}_1 - \chi_1)^2/(2\rho^2)\}}{Z} \qquad (13)$$

with Z a normalization factor. The predicted dipolar couplings for a $(\bar{\chi}_1,\rho)$ pair are given by the population-weighted averages,

$$^{1}D(\bar{\chi}_1,\rho)_{\text{calc}} = \int_{-\pi}^{\pi} p_{\bar{\chi}_1,\rho}(\chi_1)\,{}^{1}D(\chi_1)\,\mathrm{d}\chi_1 \qquad (14)$$

where the integration over χ_1 is performed numerically in 0.1° increments. Best-fit $\bar{\chi}_1$ and ρ values are obtained by minimization of a target function,

$$\chi_B^2 = \sum_{\substack{i=\text{phage,}\\ \text{bicelle}}} \sum_{k=1}^{N} \frac{(^{1}D_{\text{ex}} - {}^{1}D(\bar{\chi}_1,\rho)_{\text{calc}})_{i,k}^2}{2No_i^2} \qquad (15)$$

where the symbols have the same meaning as those in eq 12. The χ_B^2 values are plotted in Figure 6 as a function of $\bar{\chi}_1$ and ρ. From the shape of the χ^2 surface, it is obvious that the minimization is more sensitive to $\bar{\chi}_1$ than to ρ, and in some cases it is difficult to estimate ρ with high precision (i.e., detect small amounts of dynamic averaging). Nonetheless, many of

Table 1. Summary of Model Parameters

I. β-Methylene-Containing Residues

	model A		model B				model C						
res[a]	χ_1[b]	χ_A^2[c]	$\bar{\chi}_1$[d]	ρ[e]	χ_B^2[f]	p[g]	$\chi_1(g+)$[h]	$\chi_1(tr)$[h]	$\chi_1(g-)$[h]	P_{g+}[j]	P_{tr}[j]	P_{g-}[j]	N[k]
K5[i]	−41.9	1538	−47.8	30.0	316	0.11	***63(13)***	***−154(11)***	***−52(6)***	***0.15(0.07)***	***0.29(0.05)***	***0.56(0.04)***	***3375***
K5[ii]	−40.8	1657	−45.6	30.0	729	0.27	***71(13)***	***−178(5)***	***−66(8)***	***0.11(0.06)***	***0.49(0.04)***	***0.40(0.04)***	***12637***
N7[i]	−57.6	204	−59.1	17.7	23	0.06							0
N7[ii]	176.0	255	180.0	20.4	50	0.13							0
L8[i]	−57.9	135	−61.0	15.9	50	0.43	97(4)	−175(12)	−60(1)	0.15(0.01)	0.01(0.01)	0.83(0.01)	91
L8[ii]	−173.6	74	−173.8	11.2	40	0.32							0
F10[i]	−59.4	19	−59.7	4.8	19	0.91							0
F10[ii]	173.7	1481	173.7	0.0	1481	1.00							0
N12[i]	64.4	18	64.4	0.0	18	1.00							0
N12[ii]	76.0	907	−168.7	30.0	807	1.00							0
S14[i]	58.5	668	60.7	30.0	111	0.09	***65(6)***	***165(17)***	***−52(13)***	***0.60(0.04)***	***0.20(0.07)***	***0.20(0.04)***	***2174***
S14[ii]	39.8	1125	32.8	30.0	472	0.46							0
F20[i]	−65.2	25	−65.2	0.0	25	1.00							0
F20[ii]	−35.0	1493	−94.3	30.0	1385	1.00							0
K21[i]	−99.4	292	−90.5	30.0	107	0.24	***71(11)***	***−176(12)***	***−63(4)***	***0.14(0.01)***	***0.19(0.01)***	***0.67(0.01)***	***15056***
K21[ii]	16.7	257	20.9	27.8	111	0.25							0
Y32[i]	−69.3	173	−69.0	11.9	168	0.84	62(10)	141(2)	−75(1)	0.01(0.01)	0.17(0.01)	0.81(0.00)	9
Y32[ii]	−72.4	1860	95.0	30.0	1479	1.00							0
Y34[i]	178.8	8	−179.7	11.5	2	0.14							0
Y34[ii]	−86.4	1922	−86.4	0.0	1922	1.00							0
D36[i]	−173.0	1552	−172.2	21.4	1360	1.00							0
D36[ii]	−79.7	61	−80.4	10.5	48	0.54							0
L38[i]	−67.1	43	−66.6	10.9	25	0.35	51(23)	169(4)	−68(0)	0.01(0.01)	0.08(0.00)	0.91(0.01)	544
L38[ii]	−166.6	1727	−148.2	30.0	538	1.00							0
K39[i]	−89.7	559	−85.7	30.0	265	0.27	***75(10)***	***178(10)***	***−61(6)***	***0.24(0.03)***	***0.31(0.03)***	***0.45(0.03)***	***13081***
K39[ii]	−106.4	1038	21.6	30.0	164	0.16	43(6)	−170(14)	−50(12)	0.55(0.04)	0.15(0.03)	0.31(0.03)	525
D41[i]	−58.8	189	−68.2	29.1	64	0.19							0
D41[ii]	−165.7	885	−165.7	0.0	885	1.00							0
N42[i]	−56.7	3	−56.7	0.0	3	1.00							0
N42[ii]	−14.0	3685	−14.0	0.0	3685	1.00							0
E44[i]	66.9	60	66.7	16.8	32	0.32	***77(3)***	***−171(7)***	***−74(22)***	***0.58(0.04)***	***0.34(0.04)***	***0.07(0.05)***	***2010***
E44[ii]	−177.6	179	−177.4	27.1	66	1.00							0
W45[i]	58.2	58	58.2	0.0	58	1.00	53(1)	−169(4)	−74(8)	0.81(0.01)	0.14(0.01)	0.05(0.01)	700
W45[ii]	−65.2	874	168.4	30.0	487	1.00							0
D48[i]	10.7	2752	15.1	30.0	715	0.40							0
D48[ii]	148.7	1122	148.8	30.0	306	0.15	***64(10)***	***−167(7)***	***−69(5)***	***0.01(0.01)***	***0.47(0.01)***	***0.52(0.01)***	***15690***
D51[i]	−59.6	210	−60.9	22.4	22	0.05							0
D51[ii]	−161.6	632	−161.3	10.9	622	1.00							0
Y54[i]	−62.1	13	−63.1	7.1	12	0.81							0
Y54[ii]	77.7	2022	77.7	0.0	2022	1.00							0
L56[i]	−59.2	52	***−60.2***	***14.1***	***0***	***0.00***	***38(15)***	***−174(11)***	***−60(1)***	***0.06(0.01)***	***0.01(0.01)***	***0.93(0.01)***	***1704***
L56[ii]	167.2	696	170.9	22.3	360	1.00							0
N57[i]	−63.4	58	−63.7	11.1	21	0.21							0
N57[ii]	−169.3	686	−168.3	12.2	638	1.00							0
K59[i]	−14.5	511	−12.2	30.0	176	0.19	63(13)	−179(10)	−28(4)	0.20(0.02)	0.23(0.03)	0.57(0.04)	301
K59[ii]	143.6	1014	141.8	30.0	639	1.00	***69(12)***	***−163(6)***	***−52(4)***	***0.05(0.02)***	***0.46(0.01)***	***0.49(0.02)***	***4129***

II. β-Methine-Containing Residues

	model A		model B			model C						
res	χ_1[b]	χ_A^2[c]	$\bar{\chi}_1$[d]	ρ[e]	χ_B^2[f]	$\chi_1(g+)$[l]	$\chi_1(tr)$[l]	$\chi_1(g-)$[l]	P_{g+}[m]	P_{tr}[m]	P_{g-}[m]	N[n]
V2	−50.0	8	−48.9	12.4	5×10^{-3}	61(7)	177(9)	−46(4)	0.19(0.10)	0.13(0.11)	0.68(0.17)	228
T3	−63.3	66	−59.7	16.6	1×10^{-3}	66(9)	−168(6)	−61(2)	0.06(0.03)	0.03(0.02)	0.91(0.02)	275
I9	−74.2	79	−64.2	19.6	2×10^{-3}	61(5)	−173(21)	−59(2)	0.06(0.04)	0.07(0.04)	0.87(0.02)	407
T15	−165.5	4	−165.5	0.0	4	***54(6)***	***−166(6)***	***−53(10)***	***0.21(0.11)***	***0.66(0.18)***	***0.13(0.09)***	***2605***
T17	−112.1	85	−113.1	3.0	80	***59(6)***	***−169(6)***	***−56(7)***	***0.33(0.08)***	***0.11(0.08)***	***0.56(0.01)***	***2170***
T28	−7.6	11	−69.1	24.2	4×10^{-4}	64(9)	−170(6)	−57(8)	0.28(0.11)	0.19(0.09)	0.53(0.16)	1327
T37	−67.4	11	−67.4	0.0	10	***74(5)***	***−169(6)***	***−67(7)***	***0.60(0.18)***	***0.11(0.07)***	***0.30(0.24)***	***665***
T46	6.8	103	6.8	0.0	100	***56(5)***	***−168(7)***	***−60(9)***	***0.74(0.08)***	***0.12(0.03)***	***0.14(0.10)***	***556***
V47	56.5	123	74.9	3.0	6×10^{-3}	66(5)	175(10)	−64(8)	0.80(0.03)	0.15(0.06)	0.05(0.03)	322
V49	−177.5	311	176.8	27.3	1×10^{-3}	69(10)	175(3)	−64(9)	0.14(0.07)	0.80(0.04)	0.06(0.03)	354
T55	−63.8	15	−62.6	1.0	1×10^{-3}	65(10)	−169(6)	−63(0)	0.02(0.01)	0.02(0.01)	0.96(0.01)	122

[a] (i) and (ii) refer to stereospecific assignment and are related by exchanging dipolar coupling data for $H^{\beta 2}$ and $H^{\beta 3}$. [b] Best-fit value of dihedral angle χ_1 for static model. [c] Minimum χ_A^2 at best-fit χ_1 value defined by eq 12. [d] Best-fit mean χ_1 dihedral angle for Gaussian axial fluctuation model. [e] Best-fit standard deviation of χ_1 for Gaussian axial fluctuation model. [f] Minimum χ_B^2 defined by eq 15. [g] Probability that the reduction in χ^2 from the fit using model B relative to model A is due to chance. The lesser of $(\chi^2_{A,i},\chi^2_{A,ii})$ is compared to both $(\chi^2_{B,i},\chi^2_{B,ii})$. Residues with $p \le 0.01$ are in bold italics. [h,j] Mean (standard deviation) χ_1 dihedral angles and mean (standard deviation) relative populations of $\chi_1 \approx (60°,180°,-60°)$ (g+,tr,g−) rotamers for Monte Carlo iterations with $\chi_C^2 \le \chi_A^2/50.5$ ($p \le 0.01$) assuming a three-site jump model. χ_C^2 is defined by eq 16. The lesser of $(\chi^2_{A,i},\chi^2_{A,ii})$ is compared to both $(\chi^2_{C,i},\chi^2_{C,ii})$. [k] Number of Monte Carlo iterations with statistical significance, $p \le 0.01$ ($N > 1000$ are in bold italics). [l,m] Mean (standard deviation) χ_1 dihedral angles and mean (standard deviation) relative populations of $\chi_1 \approx (60°,180°,-60°)$ (g+,tr,g−) rotamers for Monte Carlo iterations with $\chi_C^2 < 10^{-3}$ assuming a three-site jump model. Residues for which models A and B are not appropriate are in bold italics. [n] Number of Monte Carlo iterations with $\chi_C^2 < 10^{-3}$.

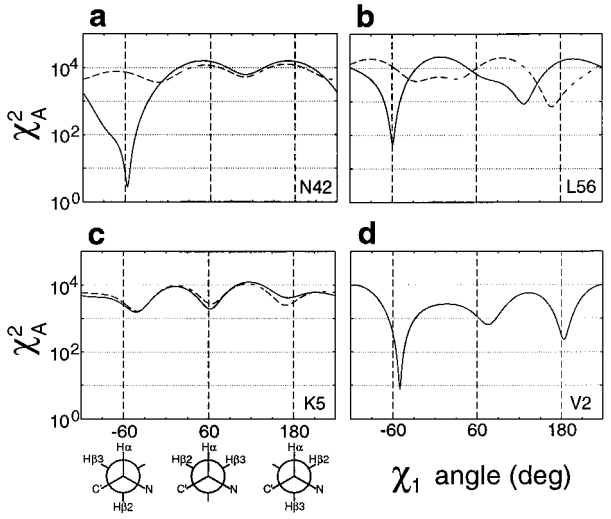

Figure 5. χ^2_A (eq 12) obtained from model A (no motion about the χ_1 dihedral angle) as a function of χ_1 for (a) N42, (b) L56, (c) K5, and (d) V2. Solid and dashed lines correspond to alternate stereoassignments (i) and (ii), respectively, which are obtained by exchanging data for $H^{\beta 2}$ and $H^{\beta 3}$.

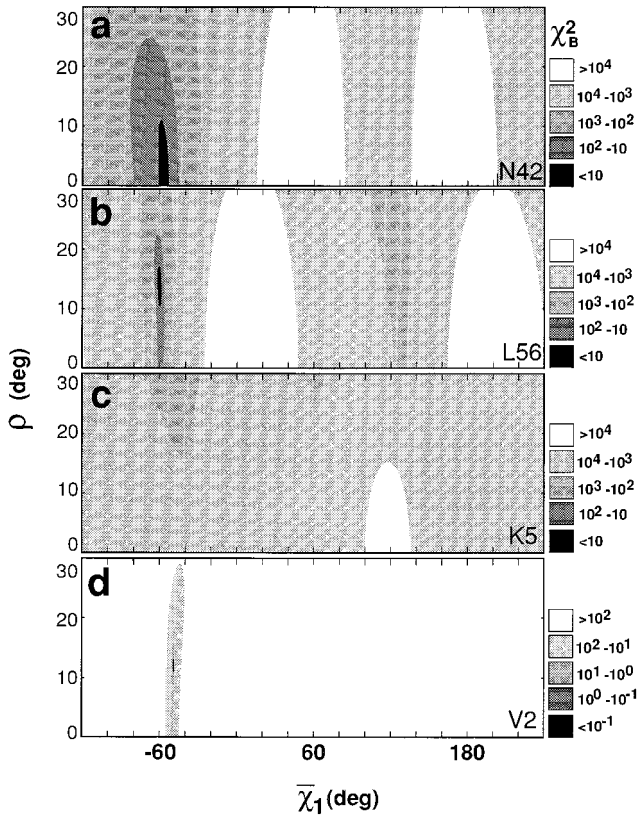

Figure 6. χ^2_B (eq 15) obtained from model B (Gaussian axial fluctuation model) as a function of $\bar{\chi}_1$ (mean) and ρ (standard deviation) of χ_1 dihedral angles for (a) N42, (b) L56, (c) K5, and (d) V2. Only the stereoassignments corresponding to the solid lines in Figure 5 (i) are included.

the ($\bar{\chi}_1$,ρ) parameters calculated by this method compare well with the corresponding values observed in high-resolution crystal structures.[41] For example, Y34 is best fit by a distribution of χ_1 angles with a mean of $-179.7°$ and standard deviation, $\rho = 11.5°$. The distribution of χ_1 angles reported by Ponder and Richards for tyrosine residues in the trans conformation has a mean of $-179.7°$ and a standard deviation of 12.6°.

For residues with two β protons, four $^{13}C^{\beta}-^{1}H^{\beta}$ dipolar couplings are measured (two per alignment media), and in models A and B there are therefore three and two degrees of freedom, respectively. In what follows, model B is said to afford a statistically significant improvement in fit relative to model A if $p \leq 0.01$ (see Materials and Methods), corresponding to a 50.5-fold decrease in χ^2. Of all the residues considered here, only L56 (Figure 6b) shows a reduction of such magnitude. This is a consequence of the shallow profile of χ^2 as a function of ρ (Figure 6), so that even a relatively mobile residue can often be well fit assuming a single orientation with $\rho = 0$. Conversely, residues such as K5 (Figure 6c) which are poorly fit using model A show little improvement with the addition of small-amplitude averaging within a well.

In the case of a single β proton, there are no degrees of freedom for model B, and the F statistic of eq 5 is undefined. For these residues, model B is considered acceptable so long as $\chi^2 \approx 0$. Seven of the 11 residues have residual χ^2 values on the order of 10^{-3} (compared with 10^1-10^2 for method A), suggesting that this model is appropriate in these cases. In contrast, fits involving the remaining residues, T15, T17, T37, and T46, have much larger χ^2 values, between 1 and 100, and these amino acids are analyzed in the context of a rotamer-jump model described next. Of interest, the values of $\bar{\chi}_1$ obtained for residues with a single β proton that are well fit using model B are in better agreement with the crystal structure than χ_1 values obtained using model A (7.2° vs 11.0° rmsd from mean crystal structure values). In particular, a physically unlikely value for χ_1 ($-7.6°$) is predicted for T28 using model A, while with model B, $\bar{\chi}_1 = -69.1°$. This value compares very favorably with χ_1 angles of $-65.7°$, $-62.8°$, and $-65.0°$ obtained for T28 from the three copies of the structure in the asymmetric unit.

Model C. The third model considers discrete jumps between the three canonical rotamers with jump rates that are large compared to the $^{13}C^{\beta}-^{1}H^{\beta}$ dipolar couplings. In essence, this model contains five parameters: three dihedral angles (χ_1(g+), χ_1(tr), χ_1(g−)) that are close but in general not equal to 60°, 180°, and −60°, respectively, and two relative rotamer populations (P_{g+}, P_{tr}). The third population can be calculated from the other two since their sum is unity. A simple minimization with respect to all five parameters would constitute an overfitting of the data. Instead, we chose to hold the χ_1(g+,tr,g−) parameters fixed to physically reasonable values and fit rotamer populations by minimizing a target function,

$$\chi^2_C = \sum_{\substack{i=\text{phage,}\\ \text{bicelle}}} \sum_{k=1}^{N} \frac{\{{}^1D_{ex} - \sum_{n=g+,g-,tr} P_n\, {}^1D(\chi_1(n))_{calc}\}^2_{i,k}}{2N\sigma_i^2} \qquad (16)$$

where symbols are defined as in eq 12. Since there are fairly broad distributions of reasonable χ_1 values, we have adopted a Monte Carlo approach in which values of χ_1(g+,tr,g−) are chosen at random from residue-specific Gaussian distributions constructed on the basis of a high-resolution crystal structure database.[41] The extent to which the distribution of χ_1 values affects the fitted rotamer populations is reflected by the widths of the resultant distributions, listed in Table 1. As in model B, a 50.5-fold reduction in χ^2 relative to fits using model A is chosen as the criterion for significant improvement, corresponding to $p = 0.01$. Since there is a 1% probability that model C affords a significant improvement over model A by chance, model C is chosen only if a 50.5-fold reduction in χ^2 is observed in more than 1% of the Monte Carlo trials (i.e., in at least 1001 trials out of 100 000 performed). In our analysis, this was

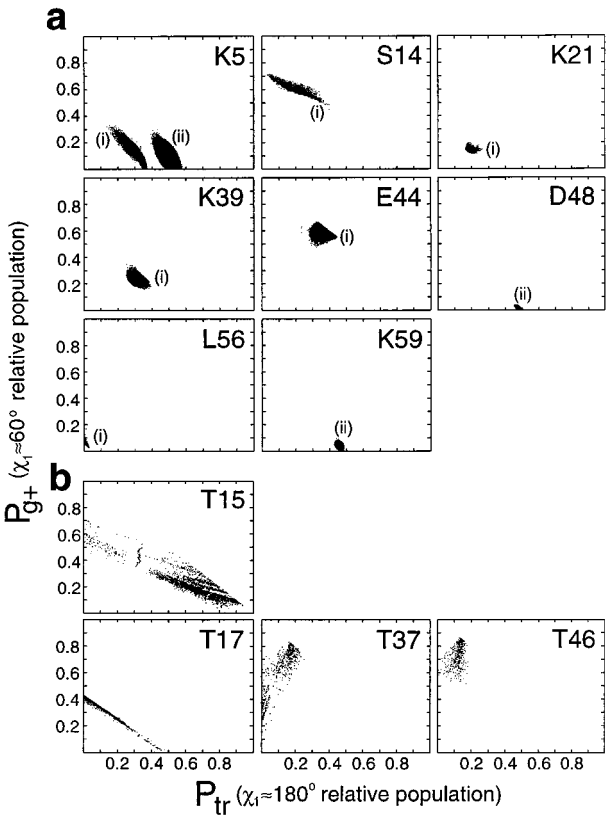

Figure 7. Relative populations of $\chi_1 \approx 180°$ (P_{tr}) and $\chi_1 \approx 60°$ (P_{g+}) rotamers for residues containing (a) two and (b) one β proton that are best fit by rotameric jumps between g+, g−, and tr χ_1 values. The relative population of the $\chi_1 \approx -60°$ rotamer (P_{g-}) can be calculated as $1 - (P_{g+}) - (P_{tr})$. Each point represents the best-fit rotamer populations obtained in a Monte Carlo iteration with random selection of $\chi_1(g+)$, $\chi_1(g-)$, and $\chi_1(tr)$ in accord with distributions reported for high-resolution crystal structures.[41] Labels (i) and (ii) refer to the two stereoassignments corresponding to solid and dashed lines, respectively, in Figure 5. Only points with $\chi_C^2 \leq \chi_A^2/50.5$ (a) and $\chi_C^2 < 10^{-3}$ (b) are shown, as discussed in the text. In (a), only residues having more than 1000 Monte Carlo iterations with $\chi_C^2 \leq \chi_A^2/50.5$ are included.

observed for eight β-methylene-containing residues, and four of them showed at least a 50.5-fold decrease in χ^2 in over 10 000 trials. The (P_{g+},P_{tr}) relative populations for these eight residues are plotted in Figure 7a, including only trials with $p \leq 0.01$. Resultant clusters are very compact, with mean standard deviations in populations of 3%. The labels (i) and (ii) adjacent to the distributions refer to the two possible stereospecific assignments of the β-methylene protons. In almost all cases, only one assignment provides a significant improvement in fit over model A, so that stereoassignments are obtained simultaneously with rotamer populations. The remaining 15 residues show large reductions in χ^2 much less frequently than would be predicted if model C were appropriate. Of the eight β-methylene-containing residues well fit by the jump model (model C), only L56 can be well fit using model B. Both models B and C predict the same stereospecific assignment (i) and a principal value of $\chi_1 \approx -60°$ ($\bar{\chi}_1 = -60.2°$, model B; $P_{g-} = 0.93$, mean $\chi_1(g-) = -60 \pm 1°$, model C). Since L56 is buried within the hydrophobic core of the protein,[38] steric considerations would suggest that model B is more likely to be correct. In the discussion that follows, therefore, L56 is not included with the group of residues that are best fit using model C (K5, S14, K21, K39, E44, D48, K59, T15, T17, T37, and T46).

For residues with only a single H^β, an *F*-statistic test cannot be used since the number of degrees of freedom for model C is zero. In this case, residues which are not well fit by model B (T15, T17, T37, and T46) are considered candidates for the rotamer-jump model. In 100 000 Monte Carlo iterations analogous to the ones described above, a small fraction have $\chi_C^2 < 10^{-3}$. Notably, the four residues which are most poorly fit by the Gaussian averaging model (model B) are among the five best fit by model C (largest number of trials with $\chi_C^2 < 10^{-3}$). Pairs of (P_{g+},P_{tr}) values for iterations with $\chi_C^2 < 10^{-3}$ are shown in Figure 7b. These distributions are significantly less compact than those for residues with two β protons (mean standard deviation in population values of 10%); however, clear preferences do emerge.

Discussion

Pulse schemes for measuring individual one-bond $^{13}C-^1H$ dipolar couplings applicable to both CH and CH_2 moieties in ^{13}C-labeled, ~50% random fractionally deuterated proteins have been described. Of note, in a related approach Tjandra et al. have recently prepared ^{15}N,^{13}C-labeled DNA, where many of the nucleotides were deuterated at the H2′ and H5′ positions, facilitating measurement of individual $^{13}C-^1H$ couplings in methylene groups.[49] Recently, Griesinger and co-workers have presented experiments for measuring $^1D_{CH}$ and $^2D_{HH}$ dipolar couplings in methylene groups in proteins and have measured $^{13}C^\alpha-^1H^\alpha$ couplings at Gly positions in ubiquitin.[50] In the present study, $^{13}C^\beta-^1H^\beta$ dipolar couplings for 25 of 35 β-CH_2 and 13 of 14 β-CH groups in protein-L were obtained for two distinct alignment frames. In addition, $^{13}C^\alpha-^1H^\alpha$, $^{13}C^\alpha-^{13}C^\beta$, and $^{13}C^\alpha-^{13}C'$ dipolar couplings were measured. The correlation between measured backbone couplings and those predicted from the X-ray crystal structure[38] is poor, suggesting subtle but important differences in orientations of backbone bond vectors in solution and X-ray states. In general, rotations of 10° or less are sufficient to generate the solution orientations of fragments (each fragment is centered at C^α and comprised of C^α, C^β, H^α, and C′ atoms), as indicated by a 10-fold decrease in χ^2 between experimental and calculated dipolar couplings (see Results). The orientation of each fragment was optimized prior to the analysis of $^{13}C^\beta-^1H^\beta$ dipolar couplings in terms of χ_1 torsion angle dynamics. Three models have been used in the analysis corresponding to (i) a fixed value of χ_1 (model A), (ii) motion within a defined well (model B), and (iii) three-site jumps between χ_1 values obtained from residue-specific Gaussian distributions constructed on the basis of a high-resolution crystal structure database (model C).

For 12 β-methylene-containing residues, $^{13}C^\beta-^1H^\beta$ dipolar couplings specify both unambiguous stereoassignment and a unique value of the dihedral angle χ_1. The χ_1 angles obtained are in excellent agreement with those from the crystal structure, with an average pairwise rmsd of 5.2°. For residues with a single H^β, 7 of 11 amino acids are reasonably well fit by a single rotamer and, if averaging about a mean value is considered within the framework of a Gaussian axial fluctuation model (model B), the pairwise rmsd from crystal structure χ_1 values is 7.2°.

We have noted that dipolar couplings are not very sensitive to low-amplitude dynamics within a single rotameric potential well. Only one residue, L56, shows a statistically significant improvement in χ^2 if an additional model parameter is included to account for such motions relative to a static model (model

(49) Tjandra, N.; Tate, S.; Ono, A.; Kainosho, M.; Bax, A. *J. Am. Chem. Soc.* **2000**, *122*, 6190−6200.
(50) Carlomagno, T.; Peti, W.; Griesinger, C. *J. Biomol. NMR* **2000**, *17*, 99−109.

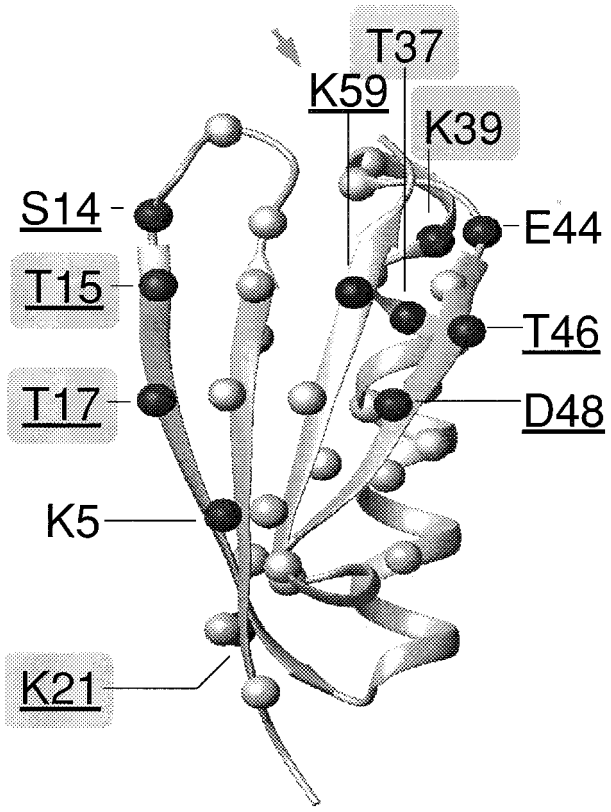

Figure 8. Structure of the B1 domain of protein-L with the C^{α} positions of residues considered in this study indicated by spheres.[38] Residues jumping between χ_1 rotamers are indicated with both labels and dark spheres (model C). Underscores identify residues with different χ_1 rotamers in the three molecules of the X-ray crystal structure. Mobile residues containing backbone amide resonances that are affected by binding to the Ig κ light-chain variable domain[26] are denoted by shaded rectangles (line-broadening) and arrows (peak shifting).

A). In contrast, seven β-methylene- and four β-methine-containing residues are best fit by a three-site rotamer-jump model (model C). The resulting relative populations are precise (to within $\pm$10% and $\pm$3% for residues containing one and two β protons, respectively) and, of interest, are somewhat correlated with the sampling of rotamers observed in the three copies of the molecule in the asymmetric unit. For example, residues S14, T15, T17, and T46 are in the g+ conformer ($\chi_1 \approx 60°$) in at least one molecule in the asymmetric unit, whereas for K21, D48, and K59, this is not the case. Average P_{g+} values obtained using model C are 0.47 and 0.07 for these two groups of residues, respectively. These residue-specific rotamer preferences are also seen in the distributions reported by Ponder and Richards.[41] Of the 11 residues found to be executing jumps about the χ_1 dihedral angle, 7, underscored in Figure 8, assume different rotameric states in the three molecules of the crystal structure. The only residue well fit by a static model but heterogeneous in the crystal structure is V47. The first and second molecules in the asymmetric unit have χ_1 values that are in agreement with the predicted χ_1 from dipolar couplings; only in the third molecule, where V47 is located at the interface with molecule 2, is a different conformation observed. The heterogeneity may therefore be a result of crystal packing forces.

A comparison of $H^{\beta 2}$ and $H^{\beta 3}$ chemical shifts reveals that those of putatively mobile residues show a smaller than average separation, which may be indicative of chemical shift averaging, consistent with dynamics. Of the eight β-CH_2-containing residues best fit using either model B or C, only for L56 are the β protons separated by more than 0.5 ppm, consistent with fluctuations within a single rotamer rather than jumping between rotamers in this case (see above).

All the residues best fit by model C are charged or polar and, with the exception of T17, are solvent accessible at the β position to a greater than average extent (>35%, see Materials and Methods for definition). It is noteworthy, however, that several charged or polar and solvent-exposed residues, N12, D36, N42, and N57, are well fit by a static model (model A). These four residues participate in side-chain hydrogen bonds with a single partner in the three molecules of the crystal structure. In contrast, such interactions are not seen for any of the mobile residues best fit using model C, with the exception of D48 and K59. Both of these residues sample different rotameric conformations in the three crystal structure molecules and hydrogen bond to different partners, depending on the value of χ_1. Thus, of the residues characterized, those with high degrees of mobility either have multiple hydrogen bonding partners or lack strong side-chain interactions altogether.

The B1 domain of protein-L binds to the variable domain of κ light chains with dissociation constants of $\sim$0.7 nM,[51] corresponding to a free energy of binding of $-$13 kcal/mol at 300 K. In light of the above discussion, it is interesting that several of the mobile residues studied in this work are implicated in binding. In a study by Wikström et al.,[26] the backbone $^{15}N-^{1}HN$ cross-peaks of 15 residues become exchange broadened in the presence of human Ig κ light-chain variable domain. Five of these residues, indicated by shaded rectangles in Figure 8, are best fit by the rotamer-jump model in this study. In addition, five resonances, including K59, shift by more than a peak width as the Ig concentration is increased. The entropic penalty for quenching the rotameric averaging of the six interfacial residues (T15, T17, K21, T37, K39, and K59) that are best fit with a jump model can be calculated from the relation[52]

$$S(\mathbf{P}) = S_0 - R\sum_n P_n \ln[P_n] \qquad (17)$$

where $S(\mathbf{P})$ is the contribution to the conformational entropy of the protein from χ_1 torsion angle dynamics, P_n is a set of nonzero jump probabilities between identically averaging rotamers, and S_0 is the conformational entropy for a single rotamer in the absence of jumps. From the values of the jump probabilities in Table 1, the penalty in free energy is 5.5*RT*, or 3.3 kcal/mol, at 300 K. Rigidification of the side chains of these residues comes at a significant cost ($\sim$25% of the binding energy), and a change in side-chain dynamics may therefore be an important mechanism for modulating overall binding energies.

The utility of dipolar couplings in structural studies of macromolecules has become well established in the past few years.[35,53,54] The present study provides a clear example of their use in the study of protein side-chain dynamics as well.

Acknowledgment. The authors are grateful to Dr. David Baker and David Kim (Department of Biochemistry, University of Washington, Seattle, WA) for providing protein-L DNA and

(51) Nilson, B. H.; Solomon, A.; Bjorck, L.; Akerstrom, B. *J. Biol. Chem.* **1992**, *267*, 2234−2239.
(52) Doog, A. J.; Sternberg, M. J. E. *Protein Sci.* **1995**, *4*, 2247−2251.
(53) Tjandra, N.; Omichinski, J. G.; Gronenborn, A. M.; Clore, G. M.; Bax, A. *Nat. Struct. Biol.* **1997**, *4*, 732−738.
(54) Prestegard, J. H. *Nat. Struct. Biol. NMR Suppl.* **1998**, *5*, 517−522.
(55) Levitt, M.; Freeman, R. *J. Magn. Reson.* **1978**, *33*, 473−476.
(56) Geen, H.; Freeman, R. *J. Magn. Reson.* **1991**, *93*, 93−141.
(57) Emsley, L.; Bodenhausen, G. *Chem. Phys. Lett.* **1987**, *165*, 469−476.
(58) Shaka, A. J.; Barker, P. B.; Freeman, R. *J. Magn. Reson.* **1985**, *64*, 547−552.
(59) Marion, D.; Ikura, M.; Tschudin, R.; Bax, A. *J. Magn. Reson.* **1989**, *85*, 393−399.

to Dr. Kam Zhang and Jason O'Neill (Fred Hutchinson Cancer Research Center, Seattle, WA) for providing the X-ray crystal structure coordinates prior to publication. They also thank Drs. Julie Forman-Kay and Nikolai Skrynnikov for helpful suggestions on the manuscript. A.M. acknowledges support in the form of a predoctroal fellowship from the Medical Research Council of Canada. This research was supported by a grant from the Natural Sciences and Engineering Research Council of Canada to L.E.K. L.E.K. is a foreign investigator of the Howard Hughes Medical Research Institute.

Supporting Information Available: Supplemental figure showing pulse schemes used to measure $^{13}C^{\alpha}-^{13}C'$, $^{13}C^{\alpha}-^{13}C^{\beta}$, and $^{13}C^{\alpha}-^{1}H^{\alpha}$ dipolar couplings (PDF). This material is available free of charge via the Internet at http://pubs.acs.org.

JA010595D